

THE PERIOD BEHAVIOUR OF THE W URSAE MAJORIS SYSTEMS  
V530 ANDROMEDAE AND V719 HERCULIS

By Christopher Lloyd

*School of Mathematical and Physical Sciences, University of Sussex*

V530 And and V719 Her are W UMa stars with two of the most extreme rates of period change, but in both cases these have been discounted. Contrary to previous results V530 And shows a small positive period change amounting to  $\dot{P} = +0.010(1) \text{ s yr}^{-1}$ , which is about an order of magnitude lower than the dispersion seen in W UMa systems. V719 Her on the other hand, in addition to being a very active system, shows a complex pattern of period behaviour with two period reversals of  $\Delta P/P = \pm 1 \times 10^{-5}$  through a series of discrete period changes between largely constant-period sections.

*Introduction*

Period changes are observed in the majority of W Ursae Majoris systems and can be attributed to light-travel-time effects due to the action of third or more bodies and/or changes due either to period reversals or apparently secular variations. Magnetic fields have a large effect on the light-curves through chromospheric activity in cooler systems, but their influence as an agent of long-term change is not clear. For systems that apparently show continuous secular changes the number showing positive or negative period changes is approximately equal with mean  $\dot{P}$  being effectively zero with a standard deviation of  $0.17 \text{ s yr}^{-1}$  from Latković *et al.*'s<sup>1</sup> sample of individual systems, and  $\sim 10^{-6} \text{ d yr}^{-1} = 0.09 \text{ s yr}^{-1}$  from Kubiak *et al.*'s OGLE sample<sup>2</sup>. The two stars discussed here have the largest negative rate of period change in Latković *et al.*'s sample at  $\dot{P} = -1.53 \text{ s yr}^{-1}$  and  $\dot{P} = -0.53 \text{ s yr}^{-1}$ , well outside the usual dispersion.

*V530 Andromedae*

V530 And is a sparsely observed, long-period,  $P = 0^d.5772$ , W Ursae Majoris system, with  $V = 12.45$  at maximum and eclipses  $0^m.6$  and  $0^m.4$  deep. The eclipses are total and it also shows a weak, positive O'Connell effect of  $\sim 0^m.01$ . The system is in marginal contact, with  $q = 0.386^{3,4}$ . The 2MASS-derived temperature  $T_{\text{eff}} = 6750 \text{ K}$  and period place the system on the boundary of the early/late-type populations of Jayasinghe *et al.*<sup>5</sup>. In a sample of 700 W UMa systems compiled by Latković *et al.*<sup>1</sup> it is listed as the system with by far the largest absolute rate of period change, with  $\dot{P} = -1.53 \pm 0.02 \text{ s yr}^{-1}$ , which is twice the size of the next-largest system. The value of  $\dot{P}$  comes from period, and wider photometric, studies by Samec *et al.*<sup>3,4</sup>, which for brevity will be later referred to as S13 and S16, respectively.

The variability of V530 And was discovered by Khruslov<sup>6</sup> in data from the Northern Sky Variability Survey (NSVS, Woźniak *et al.*<sup>7</sup>) which are no longer publicly available. Khruslov referred to the star as NSVS 6447718 and provided an ephemeris of primary minimum

$$HJD_{\text{Minl}} = 2451479.632 + 0.57723 \times E, \quad (1)$$

together with a light-curve showing the clear and unambiguous difference between the minima. The ephemeris is of relatively low precision as the *NSVS* data cover only the second half of 1999. Fitting a 6-harmonic Fourier function to the *NSVS* data with errors  $< 0^m.06$  gives an ephemeris of primary minimum of

$$HJD_{\text{Minl}} = 2451479.6354(8) + 0.577234(33) \times E, \quad (2)$$

which is consistent with Khruslov's and provides a measure of the uncertainties. Two further minima were measured by S13<sup>3</sup> in 2011, and to calculate their updated ephemeris they took nine individual faint points from the *NSVS* data and also used Khruslov's composite timing. In their second paper, S16<sup>4</sup>, they used a revised set of eight *NSVS*-derived timings and four new timings from observations made between 2013 October and 2014 January. In combination with their earlier data they constructed a quadratic ephemeris giving the large negative period change that has entered the literature.

There are very few other independent timings of V530 And. The O-C Gateway (OCG)\* lists just nine, including Khruslov's original measurement. However, these timings together with the four from S16 provide a precise linear ephemeris of primary minimum

$$HJD_{\text{Minl}} = 2451479.6316(8) + 0.57723954(8) \times E, \quad (3)$$

that is entirely consistent with Khruslov's original ephemeris, has an r.m.s. residual of  $0^d.0015$ , and does not require any period change. The only points that are inconsistent with this ephemeris are the two minima from S13<sup>3</sup> and the additional *NSVS*-derived timings they used.

The problem with the *NSVS*-derived timings is clear in their O-C diagram (see Fig. 3 of S13<sup>3</sup>), where there is a systematic difference of  $\sim 0^d.06$  between their *NSVS* timings and Khruslov's ephemeris. The reason is due to the half-day difference between JD and MJD, which is how the *NSVS* times are reported. For reasons that are not clear, all these timings, including Khruslov's time of primary minimum, are assigned as secondary minima. In their second paper Khruslov's timing is omitted and a modified set of *NSVS*-derived timings is used, but of the three that appear in the first set, all have their previous eclipse assignments changed.

The inconsistency of the two timings given by S13<sup>3</sup> comes down to a one-day error in the date. According to their paper the data were taken on 2011 September 27 and 29. However, the observations as listed in their table 1 were made during JD 245530.6–31.0 and 32.8–33.0, which correspond to 2011 September 26.1–26.5 and September 28.3–28.5. Sample FITS headers from two of these observations confirms that the HJDs as tabulated are for some unknown reason one day early (Samec, private communication). Adding one day to their timings removes this discrepancy and leads to a linear ephemeris consistent with Equation 3 with an r.m.s. residual of  $0^d.0016$ .

In an effort to increase the number of timings, additional data are taken from *Catalina Sky Survey* (CSS<sup>8</sup>), the *All-Sky Automated Survey for Supernovae* (ASAS-SN) archives<sup>9,10</sup>, and the *Asteroid Terrestrial-Impact Last Alert System* (ATLAS) project<sup>11,12</sup>. As with the *NSVS* data the times of minima have been calculated by using a 4- or 6-harmonic Fourier fit depending on the quality of

\*O-C Gateway: <http://var2.astro.cz/ocgate/index.php>

the data. The *CSS* data are taken in the *V* band and cover the years 2005–2013, but the light-curve is relatively poorly defined so they have not been divided into shorter sets, and just the one primary and secondary timing are measured for the whole interval. The *ASAS-SN* data cover the years 2012–2019 in *V* and 2016–2023 in Sloan *g*. These are divided into mostly annual sets with the poorer coverage in the early years being combined as necessary, and similarly with the *ATLAS* data which cover the years 2016–2023 in their cyan (*c*) and orange (*o*) bands. The *c* data are relatively sparse and these are combined into multi-year sets.

The system has also been observed by the *Transiting Exoplanet Survey Satellite* (*TESS*)<sup>13</sup> during 2019 November in Sector 17 at the standard 30-minute cadence, and during 2022 November in Sector 57 with a much higher cadence of 200 seconds. The data were extracted from the Full-Frame Images using the *LIGHTKURVE* package<sup>14</sup> and restricted to *HARD* quality in *LIGHTKURVE* parlance. The fluxes were measured using a slight variant of the default aperture created within the routine due to the high background and the possible contamination by two nearby stars. To help minimize this the sky background was measured in a one-pixel-wide frame, around the aperture, and this was subtracted from the target flux. The sky-subtracted flux shows the full amplitude of the light-curve and is also better corrected in the high-noise sections of data. The resulting light-curve is relatively smooth but some discordant sections were removed and additional flattening with a low-order polynomial fitting was required to correct variation in level through the *TESS* orbit, as is often the case. The *TESS* sectors naturally divide into two due to the 1–2 day break for the data downlink, so the light-curve comprises four sections of  $\sim 11$  days of mostly continuous data. The phase diagram shown in Fig. 1 is derived from an 8-harmonic Fourier fit. There is little systematic deviation from the mean light-curve and the residuals have an r.m.s. error of  $0^{\text{m}}.0075$ . The amplitudes of primary and secondary eclipses are  $0^{\text{m}}.62$  and  $0^{\text{m}}.39$  — marginally smaller than the ground-based data — and the maxima show a small O’Connell effect of  $0^{\text{m}}.01$ . Timings were calculated for every two cycles using a fixed-frequency Fourier fit and these reveal a small

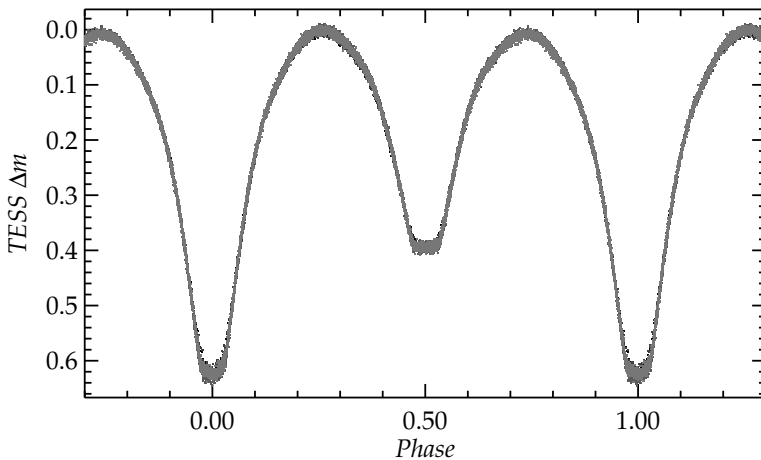


FIG. 1

The phase diagram of the *TESS* data for V530 And folded on the best-fit period derived from an 8-harmonic Fourier fit. The different half-sectors are shown in different greyscales.

TABLE I

Sample table — Times of minimum of *V*530 And from 2000 onwards

HJD	$\sigma$ (d)	Min.	Cycle	O-C (d)	Band	Data set
2451431.7243	0.0012	1	-8896.0	0.0035	R	NSVS (This paper)
2451432.0123	0.0015	2	-8895.5	0.0029	R	NSVS (This paper)
2451479.632	—	1	-8813.0	0.0003	R	NSVS Khruslov <sup>6</sup>
2451514.8466	0.0014	1	-8752.0	0.0033	R	NSVS (This paper)
2451515.1358	0.0019	2	-8751.5	0.0039	R	NSVS (This paper)
2454928.0602	0.0017	1	-2839.0	-0.0009	V	CSS (This paper)
2454928.3515	0.0035	2	-2838.5	0.0018	V	CSS (This paper)
2455831.72806	0.00045	2	-1273.5	-0.0017	UBV RI	S13 <sup>3</sup>
2455833.74595	0.00040	1	-1270.0	-0.0041	UBV RI	S13 <sup>3</sup>
2456488.33546	0.00102	1	-136.0	-0.0043	V	ASAS-SN (This paper)

This table is available at CDS by anonymous ftp to [cdsarc.u-strasbg.fr](https://cdsarc.unistra.fr/viz-bin/cat/J/other/Obs/I44.14) (130.79.128.5) or via <https://cdsarc.unistra.fr/viz-bin/cat/J/other/Obs/I44.14>

but consistent offset between the primary and secondary minima of  $0^d.0005$  for Sector 17 and  $0^d.001$  for Sector 57, with the secondary minima being slightly later. These differences probably reflect small and slow changes in the distribution of the spots found by Samec *et al.* The mean times for both minima (strictly BJD) were measured for each of the half-sectors and these are collected with all the other times of minimum in Table I, a small sample of which is given here. The difference between BJD and HJD is a few seconds and insignificant in this context.

The O-C diagram is shown in Fig. 2 and despite the large gap between the NSVS and CSS data it is obvious that there is no large period change; in fact for W UMa systems the range of variation is very modest, but it is nevertheless clear that a small, apparently secular change has occurred. The unweighted

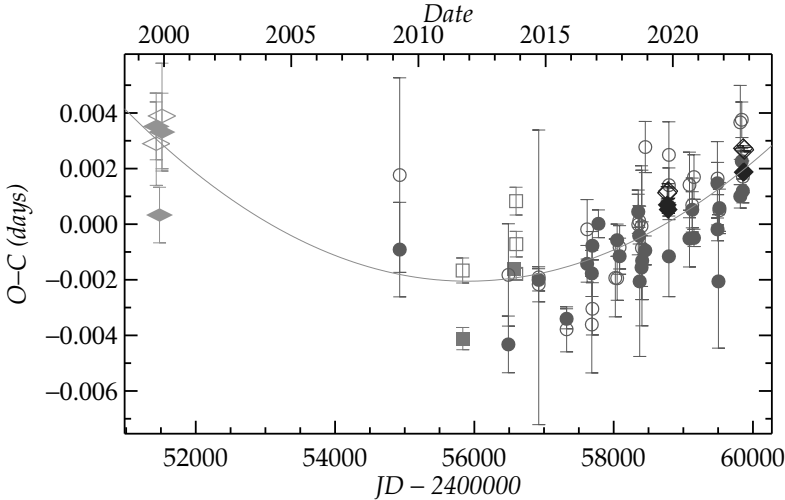


FIG. 2

The O-C diagram of *V*530 And showing two pairs of timings derived from NSVS data (lozenges) with Khruslov's  $T_0$ , the corrected S13 timings as described in the text and S16 timings (squares), the TESS data (diamonds), the OCG data and other new timings (circles) as given in Table I. Open symbols show the secondary minima. The line shows the best unweighted quadratic fit to the data as given in Equation 4.

quadratic fit to the data gives an ephemeris of primary minimum of

$$HJD_{\text{MinI}} = 2456566.84244(27) + 0.577239807(47) \times E + 8.52(88) \times 10^{-11} \times E^2, \quad (4)$$

leading to a small positive period change of  $\dot{P} = +0.010(1) \text{ s yr}^{-1}$  that is at least an order of magnitude smaller than the dispersion found in the surveys. The data cover such a short time-span and the range of the residuals is so small that it is impossible to put any constraints on the nature of the period behaviour, but any cyclical changes would require a period in excess of 30 years.

### V719 *Herculis*

V719 Her is also a relatively recent discovery but it is a star with something of a chequered history. It was identified as a likely RRab variable by Kurochkin<sup>15</sup> with  $P = 0^d.33587$ , but notes in the *GCVS* suggest that it was also considered as a *W UMa* system with twice that period. The situation was resolved by Schmidt<sup>16</sup> who found it was a *W UMa* system with  $P = 0^d.400995$ , which is the 1-day alias of the original period. The star has  $V = 12.3$  at maximum with eclipses  $0^m.55$  and  $0^m.35$  deep. The only photometric model of the system is provided by Goderya *et al.*<sup>17</sup> who find the system has  $q = 0.296$ , which is near the median for *W UMa* systems, but give a rather large value for the fillout factor,  $f = 46\%$ . They assume  $T_1 = 6580 \text{ K}$  and derive  $T_2 = 6267 \text{ K}$ , but the modern *Gaia*-derived mean value for the system is significantly cooler at  $T_{\text{eff}} = 5680 \text{ K}$ , placing the star well into the cool population of Jayasinghe *et al.*<sup>5</sup>. Goderya *et al.* also made a rather limited period study of the system based on their new data and Schmidt's earlier timing, and found a very significant period decrease amounting to  $\dot{P} = -0.54 \text{ s yr}^{-1}$ . Unfortunately, Schmidt's timing referred to maximum light as the star had originally been considered as a pulsator. Further observations by Schmidt<sup>18</sup> revealed significant variation in the shape of the light-curve and in particular the depths of the eclipses, and also showed that the new timings were not consistent with the quadratic ephemeris. All these timings have been redetermined here. Since then approximately 50 independent eclipse timings have been published and are collected by the O-C Gateway.

New minima have been calculated from the synoptic surveys *NSVS*, *CSS*, *ASAS-SN*, *ATLAS*, as above, and in this case also the *Zwicky Transient Facility (ZTF)*<sup>19</sup>, which provides good coverage from 2017 to date in the Sloan *zg* and *zr* variants. Near the maximum some of the *zr* data show saturation effects but the minima are unaffected. Timings have also been taken from the *TESS* data but these will be discussed in more detail later. The times of minima for V719 Her are listed in Table II; again a small sample is given here.

The period behaviour of V719 Her has also been investigated prior to discovery using the Harvard photographic data, which have been taken from the Digital Access to a Sky Century at Harvard (DASCH) archive\*. The data are very inhomogeneous with a relatively sparse set taken between about 1890–1930 (JD 2411000–2427000), with a much more dense set taken between about 1930–1950 (JD 2427000–2434000). A similar set of observations covers the interval from 1965–1990 (JD 2439000–2448000). When restricted to observations with errors  $< 0^m.2$  these data sets contain 129, 429, and 405 data points, respectively. None of the Harvard data are contemporaneous with any other published observations.

\*DASCH <https://library.cfa.harvard.edu/search-dasch>

TABLE II

Sample table — Times of minimum of V719 Her from 1905 onwards

HJD	$\sigma$ (d)	Min.	Cycle	O-C (d)	Band	Data set
2416588.4291	0.0044	1	-94602.0	0.0255	pg	Harvard (This paper)
2416588.6370	0.0049	2	-94601.5	0.0329	pg	Harvard (This paper)
2422894.5583	0.0052	1	-78873.0	0.0419	pg	Harvard (This paper)
2422894.7650	0.0061	2	-78872.5	0.0356	pg	Harvard (This paper)
2428985.8523	0.0034	1	-63680.0	0.0470	pg	Harvard (This paper)
2428986.0556	0.0037	2	-63679.5	-0.0441	pg	Harvard (This paper)
2432297.9125	0.0037	1	-55419.0	0.0530	pg	Harvard (This paper)
2432298.1108	0.0038	2	-55418.5	0.0552	pg	Harvard (This paper)
2442573.7768	0.0044	1	-29789.0	-0.0267	pg	Harvard (This paper)
2442573.9709	0.0047	2	-29788.5	0.0203	pg	Harvard (This paper)

This table is available at CDS by anonymous ftp to cdsarc.u-strasbg.fr (130.79.128.5) or via <https://cdsarc.unistra.fr/viz-bin/cat/J/other/Obs/144.14>

To avoid any unexpected surprises a Discrete Fourier Transform (DFT) periodogram was applied to each section to identify the dominant periods. The first set clearly showed an unambiguous peak at the anticipated half-period of the binary, but the periodogram was relatively noisy. For the other two sets a clear peak appeared at the expected frequency and in addition these DFTs show noticeable aliases at  $f \pm 0.00274 \text{ d}^{-1}$ , corresponding to a spacing of one year. The linear ephemeris was determined from the least-squares 2-harmonic Fourier fit and these are listed in Table III. Each set was divided in two and each half was fitted in the same way to determine composite times of minimum for these segments of the data. A range of initial periods were fitted and these converged to give unambiguous periods for each section. Despite the faintness of the photographic light-curves the primary minima were correctly identified in each case. Due to the sparseness of the first set an additional test was performed to estimate the reliability of the results. The set was divided in two by taking alternate points and the best fit ephemeris derived as before for each subset, and were found to be consistent.

The full O-C diagram of V719 Her is shown in Fig. 3. The photographic data cover the period from 1890–1990 and the modern data follow on directly. Although the range of the O-C residuals is relatively small there is a clear variation of period following a broadly sinusoidal period reversal. The current period is sensibly identical to the period from the early photographic data, and although it is not directly observed, the period reversal between JD 2435000 and 2440000 ( $\sim 1955$ ) is constrained to a period with a similar difference from the mean by the two shorter sections of photographic data, leading to an overall period change of  $\Delta P/P \sim 1 \times 10^{-5}$ . The period behaviour is not sinusoidal and from the detail of the recent variation shown in Fig. 4 it is more likely that there

TABLE III

Ephemerides for subsets of the data for V719 Her

Data	$T_0$	Period	Range
Harvard (Early)	2420268.910(3)	0.400924(11)	2411000 < JD < 2427000
Harvard (Middle)	2429851.453(3)	0.400927(10)	2427000 < JD < 2434100
Harvard (Late)	2445105.642(2)	0.400929(9)	2439000 < JD < 2448000
Early modern	2450284.401(2)	0.4009278(6)	2447000 < JD < 2452500
Modern	2452741.3016(4)	0.40092391(3)	2452500 < JD < 2460500
TESS	2459530.1458(3)	0.40092414(8)	2458950 < JD < 2459780

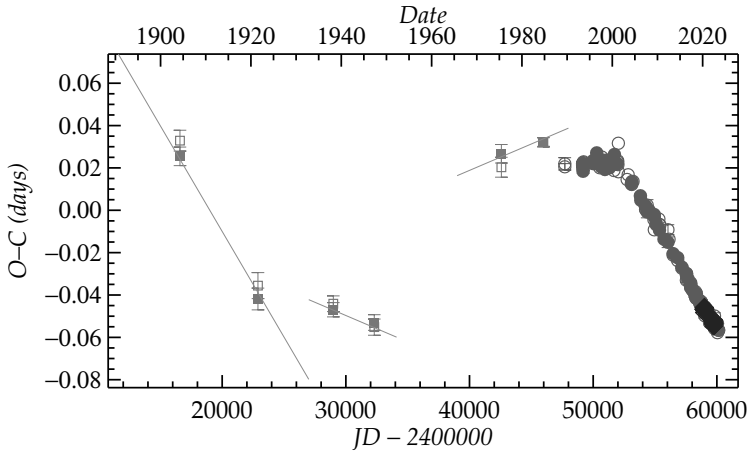


FIG. 3

The full O-C diagram of V719 Her showing the photographic data (squares), other modern data (circles), and *TESS* data (diamonds) constructed using an arbitrary ephemeris. Open symbols indicate secondary minima. The lines show the ephemerides, and extent, of the photographic data, as listed in Table III. The modern data are shown in detail in Fig. 4.

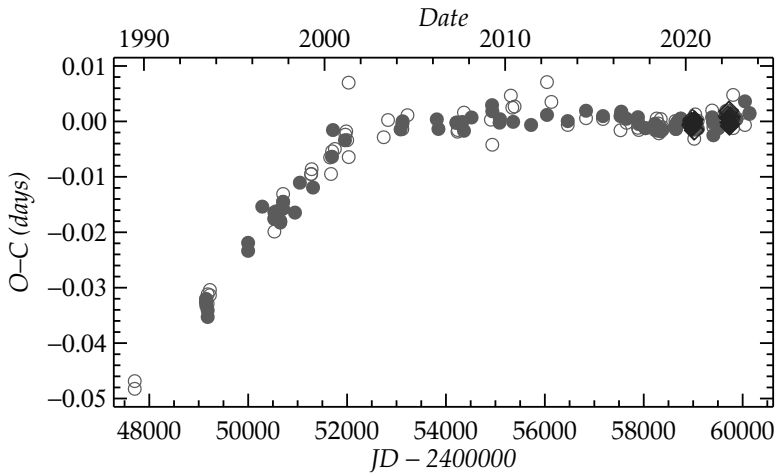


FIG. 4

The O-C diagram of V719 Her relative to the modern ephemeris, showing the modern data with the symbols as before. There is clearly a period change near JD 2452500, and some indication of a small oscillation in the most recent data. The mean periods for these sections are included in Table III.

are discrete changes between constant-period sections. The modern data are shown in detail in Fig. 4 where the most recent period change can be seen near JD 2452500 (2002), but it is also clear that the current period is not strictly constant as there is a slow oscillation, or possible prelude to another change. The behaviour between the late photographic and the early modern data

is not clear as they have very similar periods, but appear to be slightly offset. Although the interpretation in Fig. 3 appears to be the most likely, the gap in the photographic data does allow for an increase in the cycle count. In that scenario the early photographic and modern data are essentially aligned, but the overall dispersion increases to  $0^d.2$ , and to ensure continuity it requires a period change twice that necessary in Fig 3.

V719 Her was observed by *TESS* in Sectors 24, 25, and 26 during 2020 April–June at the standard 30-minute cadence and in Sectors 51, 52, and 53 during 2022 May–June at the 10-minute cadence. The flux used is the standard SAP\_FLUX from the *TESS* Science Processing Operations Center (SPOC) products, as in this case this is the most consistent of the different products that are available. All the data were used apart from two small sections from one sector where the background variation had not been correctly removed, giving 3537 observation for the first set and 10189 for the second. Each of the two sets of three consecutive sectors have approximately 80 days of near continuous data with gaps of 1–2 days between the sectors and half-sectors. The data have been folded on the ephemeris derived from an 8-harmonic Fourier fit,

$$HJD_{\text{MinI}} = 2459530.1458(3) + 0.40092414(8) \times E, \quad (5)$$

and are shown in Fig. 5. The different sectors are shaded differently and show significant variation in the depths of the eclipses and particularly in the relative heights of the maxima, in the classical O’Connell effect<sup>20,21</sup>. Between the two epochs both positive and negative O’Connell effects can be seen and the range of variation is  $\sim 0^m.05$ , and the eclipses show a similar level of variation. The maximum depths are  $0^m.55$  and  $0^m.40$ , very similar to the *R*-band data of Schmidt. Eclipse timings were calculated for every two cycles using a fixed-frequency Fourier fit and these reveal coherent movement of both the primary and secondary eclipse on a time-scale of tens of days. These are shown

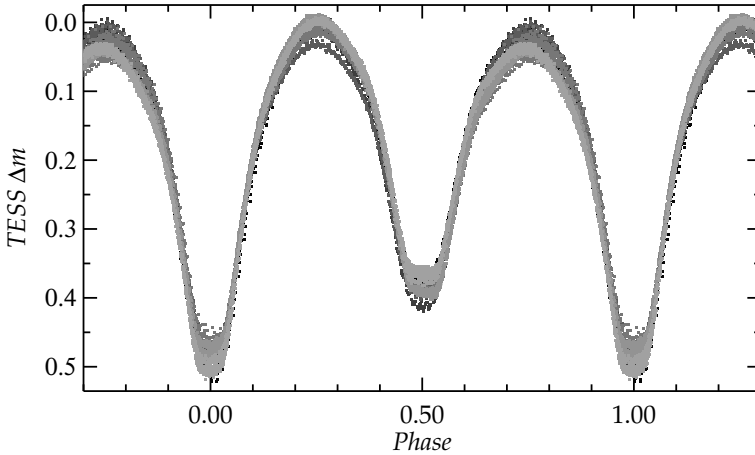


FIG. 5

The phase diagram of V719 Her showing the *TESS* data folded on the best-fit period given in Equation 5. The different sectors are shown in different symbols.

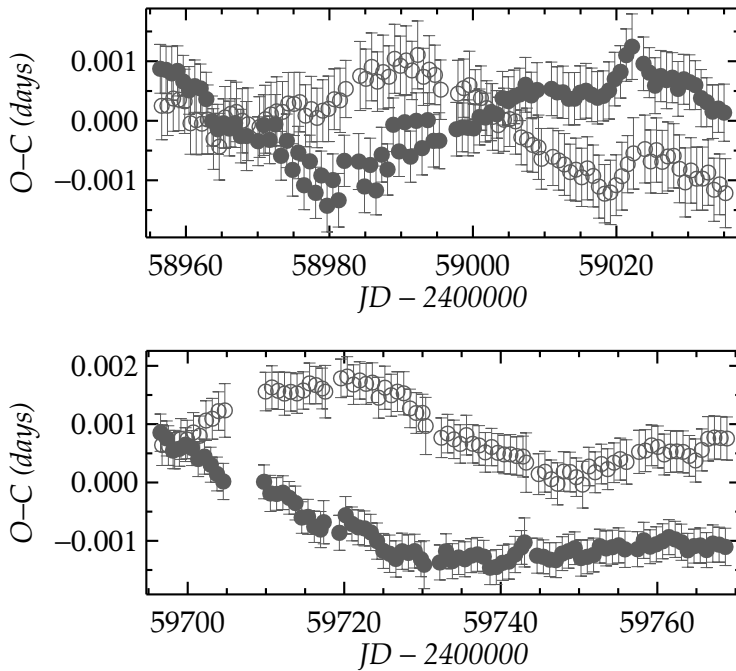


FIG. 6

The O-C diagram of V719 Her showing the timings for every two cycles of the *TESS* data relative to the *TESS* ephemeris. The top panel shows Sectors 24, 25, and 26 and the lower panel Sectors 51, 52, and 53.

for the two sets of data in Fig. 6 where for the first set the movement of the primary and secondary mirror each other, and in the second their movement is more independent. The mean times for both minima were measured for each of the half-sectors and these are collected with all the other times of minimum in Table II and Fig. 3. These variations are most likely due to the movement of spots and again the *TESS* data highlight the speed at which these changes occur. V719 Her will be observed again by *TESS* in Sectors 78–80 (2024 May–July).

### Summary

V530 And and V719 Her were originally selected in order to test the validity of the extreme rates of period change found in the literature but in both cases these have been dismissed. However, a more detailed examination of the systems has led to the discovery of a small positive period change for V530 And amounting to  $\dot{P} = +0.010(1) \text{ s yr}^{-1}$ , which is about an order of magnitude lower than the dispersion seen in *W UMa* systems. V719 Her on the other hand, in addition to being a very active system, shows a complex pattern of period behaviour.

Over the past century the system has undergone two period reversals with  $\Delta P/P = \pm 1 \times 10^{-5}$  through a series of discrete period changes between largely constant-period sections. There is some evidence in the most recent data that there are small oscillations or perturbations, meaning that the linear sections might not be truly constant. Whether this is due to the effect of active regions or a presentation of the wider behaviour is not clear at this time.

#### Acknowledgements

The author is indebted to Ron Samec for providing crucial information about the observations reported in S13. The author also appreciates helpful comments from the referee. The author is pleased to acknowledge use of NASA's Astrophysics Data System Bibliographic Services. This research has made use of the *Simbad* database and the *VizieR* catalogue-access tool, CDS, Strasbourg, France (DOI: 10.26093/cds/vizier). The author gratefully acknowledges use of the AAVSO Variable Star Index (VSX). This paper includes data collected by the *TESS* mission, which are publicly available from the Mikulski Archive for Space Telescopes (MAST). Funding for the *TESS* mission is provided by NASA's Science Mission directorate.

#### References

- (1) O. Latković, A. Čeki & S. Lazarević, *ApJ Suppl*, **254**, 10, 2021.
- (2) M. Kubiak, A. Udalski & M. K. Szymanski, *Acta Astron.*, **56**, 253, 2006.
- (3) R. G. Samec *et al.*, *ISRN Astronomy and Astrophysics*, **2013**, 201235, 2013.
- (4) R. G. Samec *et al.*, *JAVSO*, **44**, 108, 2016.
- (5) T. Jayasinghe *et al.*, *MNRAS*, **493**, 4045, 2020.
- (6) A. V. Khruslov, *Peremennye Zvezdy Prilozhenie*, **8**, 40, 2008.
- (7) P. R. Woźniak *et al.*, *AJ*, **127**, 2436, 2004.
- (8) A. J. Drake *et al.*, *ApJ*, **696**, 870, 2009.
- (9) B. J. Shappee *et al.*, *ApJ*, **788**, 48, 2014.
- (10) C. S. Kochanek *et al.*, *PASP*, **129**, 104502, 2017.
- (11) J. L. Tonry *et al.*, *PASP*, **130**, 064505, 2018.
- (12) K. W. Smith *et al.*, *PASP*, **132**, 085002, 2020.
- (13) G. R. Ricker *et al.*, *Journal of Astronomical Telescopes, Instruments, and Systems*, **1**, 014003, 2015.
- (14) Lightkurve Collaboration *et al.*, 'Lightkurve: Kepler and TESS time series analysis in Python', Astrophysics Source Code Library, record ascl:1812.013, 2018.
- (15) N. E. Kurochkin, *Peremennye Zvezdy Prilozhenie*, **3**, 201, 1977.
- (16) E. G. Schmidt, *AJ*, **102**, 1766, 1991.
- (17) S. N. Goderya, K. C. Leung & E. G. Schmidt, *Ap&SS*, **243**, 315, 1996.
- (18) E. G. Schmidt, *Information Bulletin on Variable Stars*, **4552**, 1, 1998.
- (19) F. J. Masci *et al.*, *PASP*, **131**, 018003, 2019.
- (20) D. J. K. O'Connell, *Publications of the Riverview College Observatory*, **2**, 85, 1951.
- (21) N. J. Wilsey & M. M. Beaky, *Society for Astronomical Sciences Annual Symposium*, **28**, 107, 2009.